




Article

Synthesis, Structure and NH₃ Sorption Properties of Mixed Mg_{1-x}Mn_x(NH₃)₆Cl₂ Ammines

Perizat Berdiyeva ¹, Anastasiia Karabanova ², Jakob B. Grinderslev ³, Rune E. Johnsen ²,
Didier Blanchard ², Bjørn C. Hauback ¹ and Stefano Deledda ^{1,*}

¹ Department for Neutron Materials Characterization, Institute for Energy Technology, P.O. Box 40, NO-2027 Kjeller, Norway; perizat.berdiyeva@ife.no (P.B.); Bjorn.Hauback@ife.no (B.C.H.)

² Department of Energy Conversion and Storage, Technical University of Denmark, Fysikvej, DK-2800 Lyngby, Denmark; anaka@dtu.dk (A.K.); runeejohnsen@gmail.com (R.E.J.); dibl@dtu.dk (D.B.)

³ Center for Materials Crystallography, Interdisciplinary Nanoscience Center (iNANO) and Department of Chemistry, Aarhus University, Langelandsgade 140, 8000 Aarhus C, Denmark; jakobg@inano.au.dk

* Correspondence: Stefano.deledda@ife.no; Tel.: +47-407-26-921

Received: 29 April 2020; Accepted: 28 May 2020; Published: 30 May 2020



Abstract: This paper describes the synthesis, crystal structure, and NH₃ sorption properties of Mg_{1-x}Mn_x(NH₃)₆Cl₂ ($x = 0-1$) mixed metal halide ammines, with reversible NH₃ storage capacity in the temperature range 20–350 °C. The stoichiometry (x) dependent NH₃ desorption temperatures were monitored using in situ synchrotron radiation powder X-ray diffraction, thermogravimetric analysis, and differential scanning calorimetry. The thermal analyses reveal that the NH₃ release temperatures decrease in the mixed metal halide ammines in comparison to pure Mg(NH₃)₆Cl₂, approaching the values of Mn(NH₃)₆Cl₂. Desorption occurs in three steps of four, one and one NH₃ moles, with the corresponding activation energies of 54.8 kJ·mol⁻¹, 73.2 kJ·mol⁻¹ and 91.0 kJ·mol⁻¹ in Mg_{0.5}Mn_{0.5}(NH₃)₆Cl₂, which is significantly lower than the NH₃ release activation energies of Mg(NH₃)₆Cl₂ ($E_a = 60.8$ kJ·mol⁻¹, 74.8 kJ·mol⁻¹ and 91.8 kJ·mol⁻¹). This work shows that Mg_{1-x}Mn_x(NH₃)_yCl₂ ($x = 0$ to 1, $y = 0$ to 6) is stable within the investigated temperature range (20–350 °C) and also upon NH₃ cycling.

Keywords: metal chlorides; solid solution; mixed hexammines; ammonia storage; in situ powder X-ray diffraction

1. Introduction

Energy storage materials and methods have gained high interest to ensure the transition to carbon-free future. Hydrogen, as a high-density energy carrier alternative to fossil fuels, is one of the promising solutions for energy storage systems via solid storage of hydrogen [1–4]. Several studies have highlighted the potential of ammonia for hydrogen-based energy systems [5–8].

Metal halide ammines have been studied as indirect hydrogen and ammonia storage materials [9–11]. Particularly Mg(NH₃)₆Cl₂ has received significant attention due to its high gravimetric NH₃ and H₂ capacity of 51.8 wt% and 9.2 wt%, respectively [12–17]. Mg(NH₃)₆Cl₂ crystallizes in the cubic space group $Fm-3m$ with a K₂PtCl₆-structure type and $a = 10.1899(4)$ Å [18]. NH₃ is thermally released in three steps at the temperatures of 142 °C (4 moles of NH₃), 230 °C (1 mole of NH₃) and 375 °C (1 mole of NH₃), respectively against an ammonia pressure of 1 bar [15]. The phase-formation and thermodynamic properties of Mg(NH₃)₆Cl₂, Mg(NH₃)₂Cl₂ and Mg(NH₃)Cl₂ have been thoroughly studied, and the high temperatures necessary to release the two last moles of NH₃ hampers the application of Mg(NH₃)₆Cl₂ as an effective energy storage system [19–22]. However, the desorption temperatures of NH₃ may be tailored toward lower NH₃ desorption temperatures via the formation of

solid solutions, e.g., mixed cation metal halide amines. $\text{Mn}(\text{NH}_3)_6\text{Cl}_2$ also exhibits a high gravimetric capacity of ammonia (44.8 wt%), and is isostructural to $\text{Mg}(\text{NH}_3)_6\text{Cl}_2$ with a slightly larger unit cell parameter: $a = 10.249(3) \text{ \AA}$ [23]. Similar to $\text{Mg}(\text{NH}_3)_6\text{Cl}_2$, NH_3 is released from $\text{Mn}(\text{NH}_3)_6\text{Cl}_2$ in three steps with desorption temperatures of 80 °C, 180 °C, and 354 °C, respectively, and thus lower than the desorption temperatures of $\text{Mg}(\text{NH}_3)_6\text{Cl}_2$ [13,15]. However, only the sorption cyclability of the four first moles of NH_3 in $\text{Mn}(\text{NH}_3)_6\text{Cl}_2$ has been considered for ammonia storage applications, which is found to be reversible for at least 10 cycles [10].

The ammonia release temperatures are associated with the binding energy of NH_3 with its surrounding ions, which depends on the elements and crystal structures of the metal halides as elucidated in a recent study [24]. Formation of solid solutions has been suggested as an approach to tailor the NH_3 desorption temperatures and kinetics [25–27]. The NH_3 binding energies were investigated in $\text{SrCl}_2\text{-CaCl}_2$ solid solutions, and they were found to be intermediate those of the two precursors [28]. This led to studies on solid solutions of $\text{Sr}_{1-x}\text{Ba}_x(\text{NH}_3)_8\text{Cl}_2$ and $\text{Sr}_{1-x}\text{Ca}_x(\text{NH}_3)_8\text{Cl}_2$, and their respective NH_3 release properties. $\text{Sr}_{1-x}\text{Ba}_x(\text{NH}_3)_8\text{Cl}_2$ solid solutions showed that varying the relative ratios of metal allowed tuning of the desorption temperature of ammonia. The gradual effect on the ammonia release temperature was observed with the optimal mixing condition of 37.5 % of BaCl_2 in $\text{Sr}_{1-x}\text{Ba}_x(\text{NH}_3)_8\text{Cl}_2$ showing the full release of ammonia at temperature $T < 100 \text{ °C}$ of the final mixed metal halide ammine [25]. Similarly, it was demonstrated for $\text{Sr}_{1-x}\text{Ca}_x\text{Cl}_2$ solid solutions and the corresponding $\text{Sr}_{1-x}\text{Ca}_x(\text{NH}_3)_8\text{Cl}_2$ amines that the NH_3 absorption and desorption properties could be enhanced by tuning the mixing ratio [26,27]. Additionally, the ammonia storage properties and crystal structures of the $\text{CaCl}_2\text{-CaBr}_2$, $\text{SrCl}_2\text{-SrBr}_2$ and $\text{SrCl}_2\text{-SrI}_2$ solid solutions have also been investigated, and intermediate ammonia storage properties of the mixed anion metal halides were observed [28–30]. These studies show the possibility of forming mixed metal halides with tunable ammonia sorption properties. Solid solutions of borohydride-based amines have also been investigated as potential solid-state hydrogen storage materials. The solid solutions of $\text{Mg}_{1-x}\text{Mn}_x(\text{BH}_4)_2 \cdot 6\text{NH}_3$ and structural similarities of $\text{Mg}(\text{BH}_4)_2$ and $\text{Mn}(\text{BH}_4)_2$ and their corresponding amines were studied [31,32]. Similar to the present study it revealed temperature changes for ammonia release when compared to those of the pristine samples.

Inspired by the structural similarities between $\text{Mg}(\text{NH}_3)_6\text{Cl}_2$ and $\text{Mn}(\text{NH}_3)_6\text{Cl}_2$, this work addresses an investigation of solid solutions of $\text{Mg}_{1-x}\text{Mn}_x(\text{NH}_3)_6\text{Cl}_2$. Here we show the synthesis of these novel series of mixed metal halide amines with tunable properties for the NH_3 desorption. We present the $\text{Mg}_{1-x}\text{Mn}_x(\text{NH}_3)_6\text{Cl}_2$ ($x = 0.025, 0.05, 0.1, 0.3$ and 0.5) solid solutions obtained by mechanical mixing of MgCl_2 and MnCl_2 , followed by annealing and subsequent exposure to anhydrous NH_3 gas. The mixed metal halide amines were systematically investigated with in situ powder X-ray diffraction, thermogravimetric analysis, differential scanning calorimetry and volumetric Sieverts techniques. The thermally induced ammonia release for the mixed metal halide amines is discussed: three NH_3 desorption events are observed and the crystal structures of the intermediate ammine phases are identified and structurally characterized. The kinetics, absorption, and desorption properties of NH_3 are studied. The results presented in this work show that by changing the relative Mg/Mn ratio the NH_3 sorption properties can be tuned and optimized depending on the application.

2. Materials and Methods

2.1. Sample Preparation

Anhydrous MgCl_2 and MnCl_2 powders with a purity of 99.999% were purchased from Alfa Aesar and Sigma-Aldrich, respectively. $\text{Mg}_{1-x}\text{Mn}_x\text{Cl}_2$ solid solutions ($x = 0.025, 0.05, 0.1, 0.3$ and 0.5) were obtained using a SPEX SamplePrep 8000D Dual Mixer high-energy ball mill. The powders were placed in a 25 mL hardened steel vial together with hardened steel balls (10 mm diameter) in a ball-to-powder mass ratio of 16:1 and sealed in an Ar-filled glove box ($<1 \text{ ppm}$ of O_2 and H_2O). The ball milling program was for one hour.

The as-milled powders were annealed to increase the crystallinity. Batches of ~0.5 g of the as-milled powders were sealed in a stainless-steel cylinder inside a glove box, and subsequently heated to 350 °C with a heating rate of 1 °C·sec⁻¹ and kept isothermal at 350 °C for 24 h. These samples are denoted “as-synthesized” samples. Subsequently, the as-synthesized samples were placed in a high temperature stainless-steel cylinder and connected to an in-house built Sieverts apparatus. The samples were then exposed to an NH₃ gas pressure of 2.5 bar at room temperature (RT) for at least 3 h. MnCl₂ was ammoniated for 3 h at $T = -20$ °C and 1 bar NH₃. It was then stored in a glovebox freezer at -34 °C prior to the experiments, due to instability of the Mn(NH₃)₆Cl₂ at ambient conditions. These samples are denoted “ammoniated” samples.

2.2. Thermal Analysis

Combined thermogravimetric analysis (TGA) and differential scanning calorimetry (DSC) of the monometallic and mixed metal halide amines were measured using a Netzsch STA 449 F3 Jupiter apparatus. The powders (~40 mg) were placed in an alumina crucible with a pierced lid under protective Ar atmosphere in a glove box. The alumina crucibles were shortly exposed to air (ca. 1 min) during mounting in the TGA-DSC apparatus. The powders were heated from RT to 455 °C with a heating rate of 5 °C·min⁻¹ in an Ar flow of 50 mL·min⁻¹. Additionally, the batches of Mg(NH₃)₆Cl₂, Mg_{0.5}Mn_{0.5}(NH₃)₆Cl₂ and Mn(NH₃)₆Cl₂ powder (~10 mg) were measured at six different heating rates of 1, 2, 5, 10, 20 and 40 °C·min⁻¹ for Kissinger analyses [33].

2.3. Synchrotron Radiation Powder X-ray Diffraction

High resolution in situ temperature varied synchrotron radiation powder X-ray diffraction (SR-PXD) experiments were performed at the Swiss Light Source (SLS), Switzerland and at the Diamond Light Source, Oxford, UK. At SLS, data were obtained at the Material Science powder diffraction beamline X04SA [34] using a monochromatic beam in Debye–Scherrer geometry with a Mythen microstrip detector with a wavelength of $\lambda = 0.709396$ Å. At Diamond, data were obtained at the I11 beamline [35] using a wide angle position sensitive detector and a wavelength of $\lambda = 0.82646$ Å. In both cases, the samples were loaded into 0.5 mm borosilicate glass capillaries in an Ar-filled glove box (<1 ppm of O₂ and H₂O), sealed with grease and rotated during data acquisition. The samples were heated at 5 °C·min⁻¹ from RT to 500 °C using a heat blower. The temperature was calibrated using a NaCl standard prior to diffraction runs [36]. The powder diffraction data were normalized and reduced, then modeled and refined according to the Rietveld method as implemented in the TOPAS software [37].

The structural models of Mg(NH₃)₆Cl₂, Mg(NH₃)₂Cl₂ and Ni(NH₃)Cl₂ were used as starting points for Rietveld refinements of the hexammine, diammine, and monoammine phases of the mixed metal halide amines, respectively. The diffraction peaks were modeled by a Thompson-Cox-Hastings pseudo-Voigt function. The scale factor, zero-shift, unit cell parameters, atomic positions and background were refined. The N-H and H-H distances were restrained using soft restraints function during the Rietveld refinements.

2.4. Sorption Kinetics and Cycling

The two pristine materials MgCl₂ and MnCl₂ and the mixed metal halides Mg_{0.9}Mn_{0.1}Cl₂ and Mg_{0.5}Mn_{0.5}Cl₂ ($m \sim 0.1$ g) were studied with regards to their NH₃ absorption and desorption kinetics. The absorption process was conducted under 2.5 bar of NH₃ at RT, while the desorption reaction was achieved by heating the samples up to 350 °C with a heating rate of 2 °C·min⁻¹ under 1 bar of NH₃. A calibrated volume consisting of a reference volume ($V = 482.9$ mL) and a sample chamber

($V = 23.25$ mL) was used during the experiments and the moles of absorbed and desorbed NH_3 were calculated according ideal gas law using the formula below:

$$\Delta n = \frac{\Delta PV}{RT}, \quad (1)$$

where Δn is the number of NH_3 moles absorbed or desorbed, ΔP is the pressure change in the system occurring due to absorption or desorption of NH_3 , V is the volume, R is the gas constant and T is the temperature. In all cases, the number of absorbed or desorbed moles was normalized by the molar weight of the corresponding compound. Each NH_3 desorption was followed by evacuation of the released NH_3 from the cylinder to avoid reabsorption of the NH_3 gas during cooling to RT. The NH_3 desorption/absorption was cycled four times for each sample.

3. Results and Discussion

3.1. Structural Characterization of the As-Synthesized and Ammoniated Samples at RT

SR-PXD data were collected for the pristine samples, MgCl_2 and MnCl_2 , and for the as-synthesized $\text{Mg}_{1-x}\text{Mn}_x\text{Cl}_2$, ($x = 0.025, 0.05, 0.1, 0.3$ and 0.5) samples. The unit cell parameters are presented in Table S1 in the Supporting Information. The diffraction patterns in Figure 1 confirm the formation of a MgCl_2 - MnCl_2 solid solutions, as only a single set of Bragg diffraction peaks belonging to $\text{Mg}_{1-x}\text{Mn}_x\text{Cl}_2$ are observed, which is positioned in between that of MgCl_2 and MnCl_2 . MgCl_2 and MnCl_2 are isostructural and crystallize in the trigonal CdCl_2 -type structure with space group symmetry $R\bar{3}m$ [38,39].

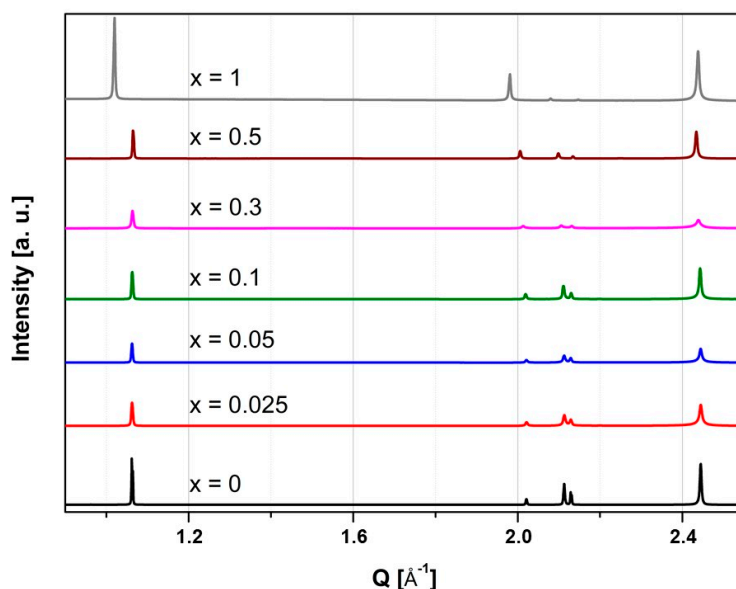


Figure 1. SR-PXD patterns of $\text{Mg}_{1-x}\text{Mn}_x\text{Cl}_2$ ($x = 0, 0.025, 0.05, 0.1, 0.3, 0.5$ and 1) obtained at RT. All peaks belong to the same CdCl_2 -type phase.

The MgCl_2 - MnCl_2 solid solution follows Vegard's law approximately, as the volume is a function of the relative content of cations and in between that of the two pristine compounds, see Figure 2a. The larger ionic radius of Mn^{2+} (0.83 Å) as compared to Mg^{2+} (0.72 Å) results in an increase of the unit cell volume [40]. The deviation from Vegard's law might be due to a localized strain field caused by difference in Mg and Mn sizes, as well as to the different outer electronic structures of the mixing components (Mg and Mn in our case) [41]. The solid solution is maintained after ammoniation and the deviation from Vegard's law remains. It should be noted that a negative deviation from Vegard's law should be also expected if contamination from iron contained in the milling media results in the form

$\text{Mg}_{1-x-y}\text{Mn}_x\text{Fe}_y\text{Cl}_2$. Indeed, the ionic radius for Fe^{2+} (0.63 Å) is smaller than the radii of both Mg^{2+} and Mn^{2+} [40]. However, even if slight contaminations from the milling media and metallic Fe cannot be ruled out, they are expected to be very limited due to the relatively short milling time (1 h) used in this work. Additionally, metallic Fe must be oxidized to Fe^{2+} in order to substitute $\text{Mg}^{2+}/\text{Mn}^{2+}$ and form $\text{Mg}_{1-x-y}\text{Mn}_x\text{Fe}_y\text{Cl}_2$. Therefore, it is most likely that the deviation from Vegard's law observed here might be due to the different outer electronic structures of Mg and Mn. Rietveld refinement and structural characterization of the ammoniated samples confirm the cubic $\text{Mg}(\text{NH}_3)_6\text{Cl}_2$ structure for all mixed cation hexammines (Supporting Information, Figure S1–S5). Figure 2b illustrate Vegard's law (blue dotted line) for $\text{Mg}_{1-x}\text{Mn}_x(\text{NH}_3)_6\text{Cl}_2$. Surprisingly, the unit cell volume for samples with $x < 0.05$ are lower than that of $\text{Mg}(\text{NH}_3)_6\text{Cl}_2$.

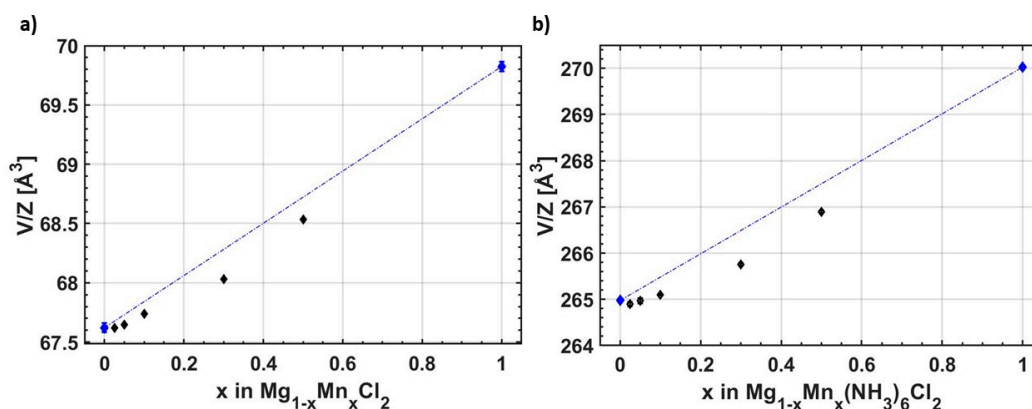


Figure 2. Unit cell volumes (V) of (a) $\text{Mg}_{1-x}\text{Mn}_x\text{Cl}_2$ and (b) $\text{Mg}_{1-x}\text{Mn}_x(\text{NH}_3)_6\text{Cl}_2$ at RT divided by the number of formula units (Z), plotted as a function of the Mn amount in the formula unit ($x = 0, 0.025, 0.05, 0.1, 0.3, 0.5$ and 1). The blue dotted line represents Vegard's law. The standard deviations are within the data points.

The atomic positions of the monometallic and mixed hexammines obtained from Rietveld refinement are presented in Table 1. During the Rietveld refinements Mg and Cl atoms are fixed in the $4a$ and $8c$ positions, respectively, while the x -coordinate of N atom ($24e$ position) is refined. N-H and H-H distances are restrained at ~ 1.107 Å and ~ 1.345 Å, respectively. Mg-N and Mn-N bond distances for the monometallic hexammines are $2.1564(7)$ Å and $2.2100(14)$ Å and thus similar to the previously reported values ($2.197(5)$ [18] and $2.270(15)$ [23], respectively). $\text{Mg}_{1-x}\text{Mn}_x$ -N bond distances are intermediate between the Mg-N and Mn-N bond distances. The unit cell parameters of the monometallic $\text{Mg}(\text{NH}_3)_6\text{Cl}_2$ and $\text{Mn}(\text{NH}_3)_6\text{Cl}_2$ obtained in this study are $a = 10.19579(9)$ Å and $a = 10.26017(2)$ Å which correspond to the values reported previously [18,23]. The unit cell parameters for $\text{Mg}_{1-x}\text{Mn}_x(\text{NH}_3)_6\text{Cl}_2$ are also intermediate between the unit cell parameters of the monometallic hexammines.

Table 1. Atomic positions of the monometallic and mixed hexammines: $\text{Mg}_{1-x}\text{Mn}_x$ ($x = 0$ to 1) in $(0, 0, 0)$, Cl in $(1/4, 1/4, 1/4)$ and N in $(x, 0, 0)^*$.

Compound	N (x -coordinate)
$\text{Mg}(\text{NH}_3)_6\text{Cl}_2$	0.21150(7), 0, 0
$\text{Mg}_{0.975}\text{Mn}_{0.025}(\text{NH}_3)_6\text{Cl}_2$	0.21268(15), 0, 0
$\text{Mg}_{0.95}\text{Mn}_{0.05}(\text{NH}_3)_6\text{Cl}_2$	0.2132(2), 0, 0
$\text{Mg}_{0.9}\text{Mn}_{0.1}(\text{NH}_3)_6\text{Cl}_2$	0.21363(8), 0, 0
$\text{Mg}_{0.7}\text{Mn}_{0.3}(\text{NH}_3)_6\text{Cl}_2$	0.21269(9), 0, 0
$\text{Mg}_{0.5}\text{Mn}_{0.5}(\text{NH}_3)_6\text{Cl}_2$	0.21267(10), 0, 0
$\text{Mn}(\text{NH}_3)_6\text{Cl}_2$	0.21540(14), 0, 0

* The data are obtained at RT.

3.2. Thermal Analysis

Figure 3 shows the TGA-DSC measurements performed on $\text{Mg}(\text{NH}_3)_6\text{Cl}_2$, $\text{Mn}(\text{NH}_3)_6\text{Cl}_2$ and $\text{Mg}_{0.5}\text{Mn}_{0.5}(\text{NH}_3)_6\text{Cl}_2$. The DSC measurements for the other mixed amines are shown in the Supporting Information (Figure S6). All the hexammine compounds are relatively stable at RT, except for $\text{Mn}(\text{NH}_3)_6\text{Cl}_2$, which slowly releases NH_3 in the glove box at RT. Thus, $\text{Mn}(\text{NH}_3)_6\text{Cl}_2$ was kept at $T = -34^\circ\text{C}$ in a glovebox freezer prior to the TGA-DSC measurements.

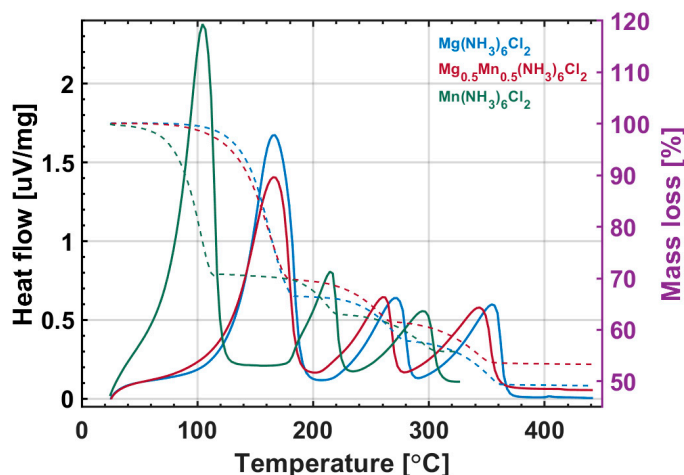


Figure 3. TGA-DSC of $\text{Mg}(\text{NH}_3)_6\text{Cl}_2$, $\text{Mg}_{0.5}\text{Mn}_{0.5}(\text{NH}_3)_6\text{Cl}_2$ and $\text{Mn}(\text{NH}_3)_6\text{Cl}_2$ measured from RT to 450°C , $\Delta T/\Delta t = 5^\circ\text{C}\cdot\text{min}^{-1}$.

TGA-DSC data shows the desorption process of the monometallic and mixed chloride amines which consists of three events. With a heating rate of $5^\circ\text{C}\cdot\text{min}^{-1}$, the onset temperatures of the initial ammonia desorption of 4 NH_3 moles from $\text{Mg}(\text{NH}_3)_6\text{Cl}_2$ and $\text{Mn}(\text{NH}_3)_6\text{Cl}_2$ are observed at 121°C and 79°C , respectively. For the solid solution $\text{Mg}_{0.5}\text{Mn}_{0.5}(\text{NH}_3)_6\text{Cl}_2$, the onset temperature for the first desorption is 116°C . The onset temperature for the next NH_3 release is at 179°C for $\text{Mg}_{0.5}\text{Mn}_{0.5}(\text{NH}_3)_2\text{Cl}_2$, significantly lower as compared to 211°C in $\text{Mg}(\text{NH}_3)_2\text{Cl}_2$ and similar to 179°C in $\text{Mn}(\text{NH}_3)_2\text{Cl}_2$. The onset temperature of the last NH_3 desorption of $\text{Mg}_{0.5}\text{Mn}_{0.5}(\text{NH}_3)_6\text{Cl}_2$ is 276°C , which is lower than the last desorption event onset temperature of $\text{Mg}(\text{NH}_3)_6\text{Cl}_2$ – 289°C . $\text{Mn}(\text{NH}_3)_6\text{Cl}_2$ starts desorbing the last mole of NH_3 at 257°C .

Each NH_3 desorption step is followed by mass loss. In the first desorption step, 4 NH_3 moles are released and $\text{Mg}_{0.5}\text{Mn}_{0.5}(\text{NH}_3)_6\text{Cl}_2$ experience a 30.2% mass loss, while the next two desorption events reduce the mass of the sample by 8.3% and 8.1%, respectively. The mass loss ratio 4:1:1 of the monometallic and mixed hexammines (Supporting Information, Table S2) corresponds to the moles of NH_3 desorbed in each desorption event, i.e., four moles of NH_3 released in the first desorption step, and 1 mole of NH_3 released in the second and third step, respectively, and agrees well with the theoretical weight loss expected from the NH_3 desorption. The gravimetric NH_3 capacities for the monometallic and the mixed cation hexammines are presented in Table S3. SR-PXD data measured of $\text{Mg}_{1-x}\text{Mn}_x(\text{NH}_3)_6\text{Cl}_2$, ($x = 0, 0.025, 0.05, 0.1, 0.3$ and 0.5) after the TGA-DSC measurements confirm the reformation of $\text{Mg}_{1-x}\text{Mn}_x\text{Cl}_2$ after full NH_3 release, thus confirming the stability of the solid solution (Supporting Information, Figure S7).

Kissinger analysis was performed on the DSC heat flow signals for the three desorption events measured for $\text{Mg}(\text{NH}_3)_6\text{Cl}_2$, $\text{Mn}(\text{NH}_3)_6\text{Cl}_2$ and $\text{Mg}_{0.5}\text{Mn}_{0.5}(\text{NH}_3)_6\text{Cl}_2$ to determine the activation energy and investigate their NH_3 desorption kinetics. Kissinger plots for the three endothermic events with the release of 4, 1 and 1 moles of NH_3 are shown in Figure 4a–c. The corresponding activation energies were calculated for each desorption event and are presented in Figure 4d–f. The activation energy of the first four moles of NH_3 desorption from $\text{Mg}_{0.5}\text{Mn}_{0.5}(\text{NH}_3)_6\text{Cl}_2$ is $54.8\text{ kJ}\cdot\text{mol}^{-1}$, which is approximately in between that of $\text{Mg}(\text{NH}_3)_6\text{Cl}_2$ ($E_a = 60.8\text{ kJ}\cdot\text{mol}^{-1}$) and $\text{Mn}(\text{NH}_3)_6\text{Cl}_2$

($E_a = 43.5 \text{ kJ}\cdot\text{mol}^{-1}$). For the second NH_3 desorption step, the activation energy for $\text{Mg}_{0.5}\text{Mn}_{0.5}(\text{NH}_3)_2\text{Cl}_2$ is $73.2 \text{ kJ}\cdot\text{mol}^{-1}$, in between that of $\text{Mg}(\text{NH}_3)_2\text{Cl}_2$ ($E_a = 74.8 \text{ kJ}\cdot\text{mol}^{-1}$) and $\text{Mn}(\text{NH}_3)_2\text{Cl}_2$ ($E_a = 67.7 \text{ kJ}\cdot\text{mol}^{-1}$). The final desorption event of $\text{Mg}_{0.5}\text{Mn}_{0.5}(\text{NH}_3)_2\text{Cl}_2$ has an activation energy of $91.0 \text{ kJ}\cdot\text{mol}^{-1}$, as compared to $\text{Mg}(\text{NH}_3)_2\text{Cl}_2$ ($E_a = 91.8 \text{ kJ}\cdot\text{mol}^{-1}$) and $\text{Mn}(\text{NH}_3)_2\text{Cl}_2$ ($E_a = 90.9 \text{ kJ}\cdot\text{mol}^{-1}$).

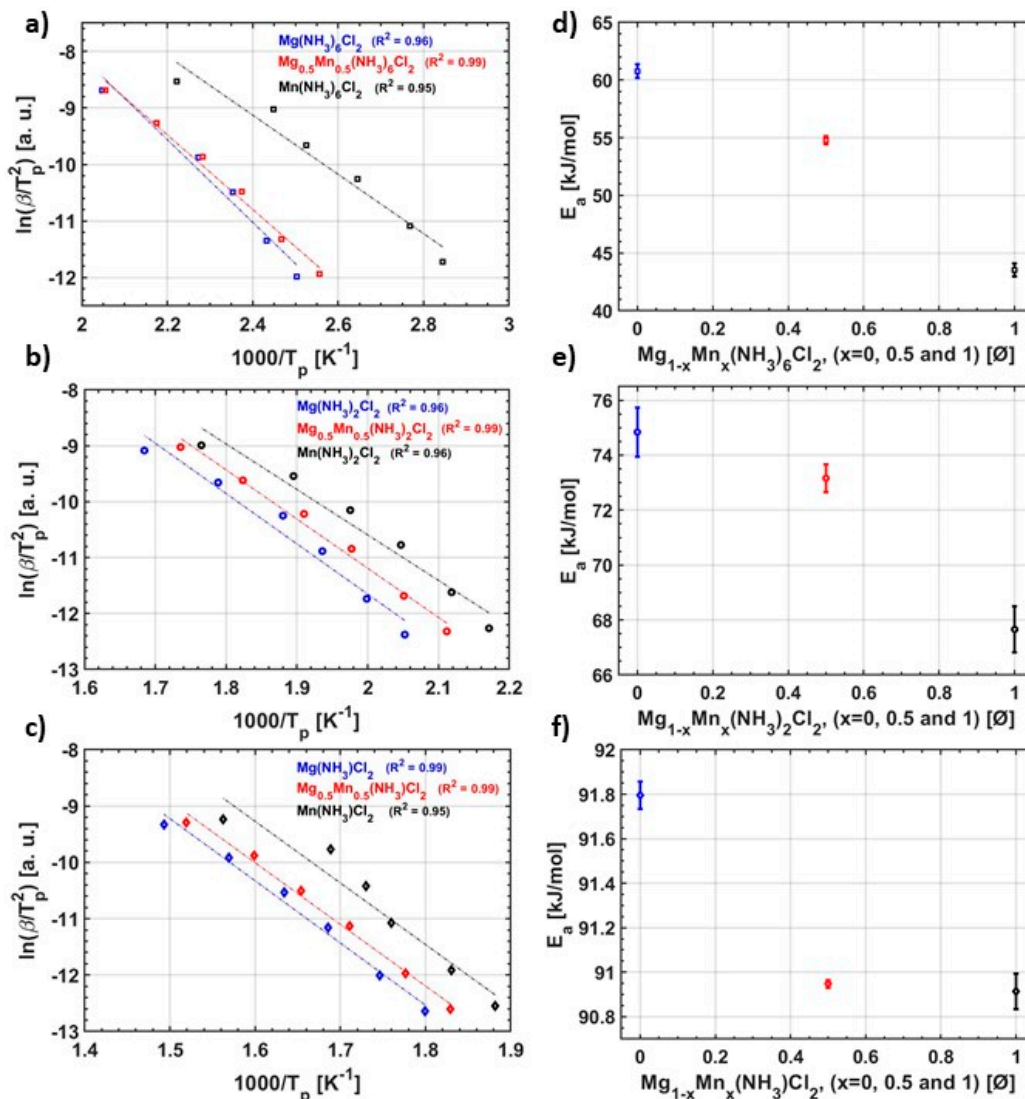


Figure 4. Kissinger analysis of the three desorption events occurring in $\text{Mg}(\text{NH}_3)_6\text{Cl}_2$ (blue), $\text{Mg}_{0.5}\text{Mn}_{0.5}(\text{NH}_3)_6\text{Cl}_2$ (red) and $\text{Mn}(\text{NH}_3)_6\text{Cl}_2$ (black). The left column (a–c) shows the Kissinger plot which corresponds to the release of (a) 4 NH_3 (b) 1 NH_3 and (c) 1 NH_3 . β is the heating rate and T_p is the corresponding peak temperature. The right column (d–f) shows the corresponding activation energies (E_a) for the three desorption events as determined by the Kissinger method. The R-values for each linear fit are included in the graphs.

The activation energies for $\text{Mg}_{0.5}\text{Mn}_{0.5}(\text{NH}_3)_6\text{Cl}_2$ in all three desorption events are significantly lower as compared to monometallic $\text{Mg}(\text{NH}_3)_6\text{Cl}_2$. Therefore, by obtaining the mixed metal halide ammines, it is possible to tailor the desorption temperature and kinetics of the mixed metal halide ammines compared to the monometallic halide ammines.

3.3. In Situ SR-PXD

The in situ SR-PXD data for $\text{Mg}_{0.5}\text{Mn}_{0.5}(\text{NH}_3)_6\text{Cl}_2$ in the temperature range RT to $402 \text{ }^\circ\text{C}$, with a heating rate of $5 \text{ }^\circ\text{C}\cdot\text{min}^{-1}$, are shown in Figure 5a, while Figure 5b shows diffraction

patterns at selected temperatures for each of the ammoniated compounds observed during heating. Rietveld refinements of the mixed metal hexammines are presented in the supporting material (Figures S1–S5). The in situ SR-PXD data from RT for monometallic $\text{Mg}(\text{NH}_3)_6\text{Cl}_2$ is shown in the supporting material (Figure S6). SR-PXD data at RT contain Bragg peaks from $\text{Mg}_{0.5}\text{Mn}_{0.5}(\text{NH}_3)_6\text{Cl}_2$ (97.6(6) wt%) and $\text{Mg}_{0.5}\text{Mn}_{0.5}(\text{NH}_3)_2\text{Cl}_2$ (2.4(5) wt%). Upon heating, the Bragg peaks corresponding to $\text{Mg}_{0.5}\text{Mn}_{0.5}(\text{NH}_3)_6\text{Cl}_2$ disappear between 115 and 125 °C, while peaks corresponding to $\text{Mg}_{0.5}\text{Mn}_{0.5}(\text{NH}_3)_2\text{Cl}_2$ increase significantly in intensity. Upon further heating, the Bragg peaks corresponding to $\text{Mg}_{0.5}\text{Mn}_{0.5}(\text{NH}_3)_2\text{Cl}_2$ decrease in intensity from ~230 °C and peaks from $\text{Mg}_{0.5}\text{Mn}_{0.5}(\text{NH}_3)\text{Cl}_2$ appear at ~246 °C. The peaks from $\text{Mg}_{0.5}\text{Mn}_{0.5}(\text{NH}_3)\text{Cl}_2$ disappear at 325 °C and some Bragg peaks from an unknown compound appear at 328 °C (Figure 5b, yellow diffraction pattern) before the full desorption of NH_3 and formation of the $\text{Mg}_{0.5}\text{Mn}_{0.5}\text{Cl}_2$ solid solution. The appearance of unknown diffraction peaks might be due to a non-stoichiometric transition from the $\text{Mg}_{0.5}\text{Mn}_{0.5}(\text{NH}_3)\text{Cl}_2$ monoammine to the $\text{Mg}_{0.5}\text{Mn}_{0.5}\text{Cl}_2$ chloride. Such behavior was previously reported for $\text{Mn}(\text{NH}_3)\text{Cl}_2$, which was observed to release the last NH_3 via two or more desorption events [13,42]. This is also observed in our data from the Sieverts measurements and will be discussed later in Section 3.4.

In situ SR-PXD data for $\text{Mn}(\text{NH}_3)_6\text{Cl}_2$ in the temperature range RT to 406 °C, with a heating rate of 5 °C·min⁻¹ confirms the presence of such intermediate phase at 307 °C (Figure S9). However, due to the fast heating rate and, therefore, dominant peaks from $\text{Mn}(\text{NH}_3)\text{Cl}_2$ and MnCl_2 phases in the diffraction pattern, it was challenging to index it and extract the unit cell parameters for $\text{Mn}(\text{NH}_3)_{1-\delta}\text{Cl}_2$. The same applies for the diffraction pattern of possible $\text{Mg}_{0.5}\text{Mn}_{0.5}(\text{NH}_3)_{1-\delta}\text{Cl}_2$ phase at 328 °C from the in situ data for $\text{Mg}_{0.5}\text{Mn}_{0.5}(\text{NH}_3)_6\text{Cl}_2$ (Figure 5), where the dominant diffraction peaks from $\text{Mg}_{0.5}\text{Mn}_{0.5}(\text{NH}_3)\text{Cl}_2$ make the indexing challenging. Observation of these intermediate diffraction patterns suggests that the transition of $\text{Mn}(\text{NH}_3)\text{Cl}_2$ to MnCl_2 and $\text{Mg}_{0.5}\text{Mn}_{0.5}(\text{NH}_3)\text{Cl}_2$ to $\text{Mg}_{0.5}\text{Mn}_{0.5}\text{Cl}_2$, which was described as non-stoichiometric process [42], in our study undergoes by stoichiometric NH_3 releases of δ moles.

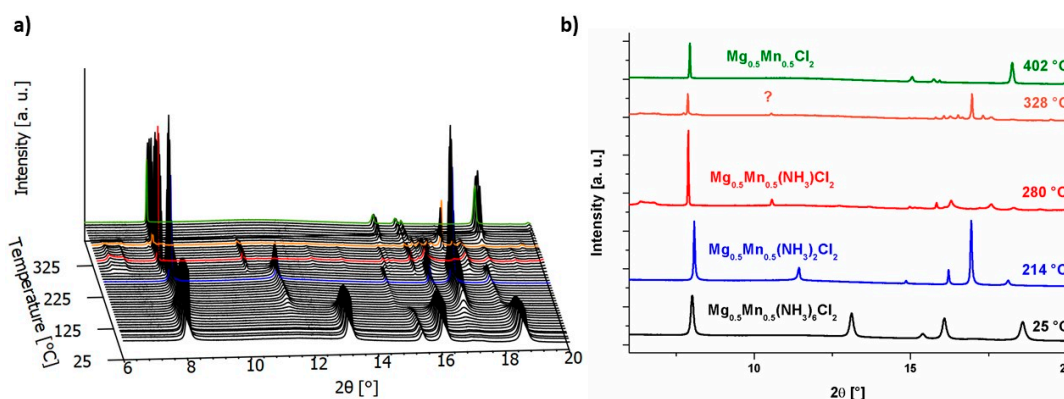


Figure 5. (a) In situ SR-PXD of $\text{Mg}_{0.5}\text{Mn}_{0.5}(\text{NH}_3)_6\text{Cl}_2$ measured from RT to 402 °C with a heating rate of 5 °C·min⁻¹ and $\lambda = 0.82646$ Å and (b) SR-PXD data at specific temperatures.

The NH_3 desorption temperatures are decreased significantly for $\text{Mg}_{0.5}\text{Mn}_{0.5}(\text{NH}_3)_6\text{Cl}_2$ as compared to monometallic $\text{Mg}(\text{NH}_3)_6\text{Cl}_2$ (Figure S8), confirming the results from TGA-DSC analysis. The first NH_3 desorption step of 4 NH_3 moles and transformation from $\text{Mg}_{0.5}\text{Mn}_{0.5}(\text{NH}_3)_6\text{Cl}_2$ to $\text{Mg}_{0.5}\text{Mn}_{0.5}(\text{NH}_3)_2\text{Cl}_2$ ($T = 125$ °C) is 20 °C lower than observed for $\text{Mg}(\text{NH}_3)_6\text{Cl}_2$ ($T = 146$ °C). All NH_3 is desorbed from $\text{Mg}_{0.5}\text{Mn}_{0.5}(\text{NH}_3)_6\text{Cl}_2$ at $T = 337$ °C, significantly lower than reported for $\text{Mg}(\text{NH}_3)_6\text{Cl}_2$ ($T = 375$ °C) [15]. The first desorption step of $\text{Mg}(\text{NH}_3)_6\text{Cl}_2$ at 146 °C is similar to the temperature reported in the literature ($T = 142$ °C) [15].

Rietveld refinements of the hexa-, di-, monoammine and chloride are shown in Figure 6, and Table 2 summarizes their structural information.

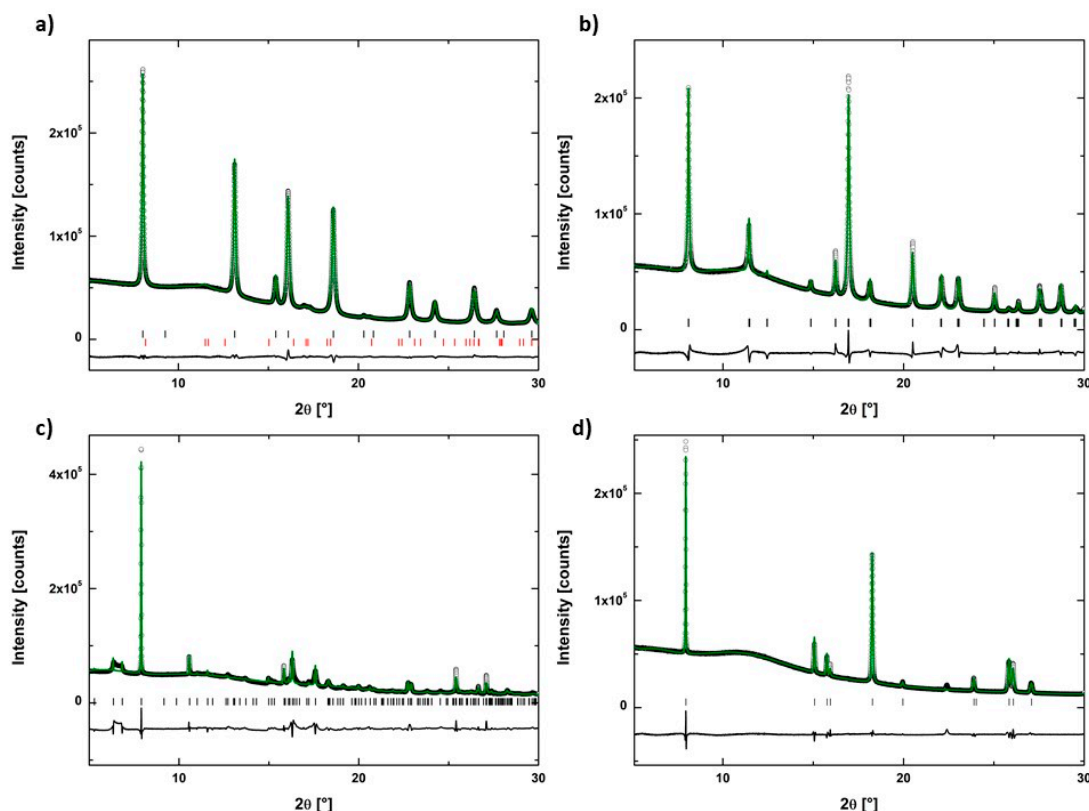


Figure 6. Rietveld refinements of the SR-PXD data for (a) $\text{Mg}_{0.5}\text{Mn}_{0.5}(\text{NH}_3)_6\text{Cl}_2$ at RT ($R_{\text{wp}} = 1.48\%$), (b) $\text{Mg}_{0.5}\text{Mn}_{0.5}(\text{NH}_3)_2\text{Cl}_2$ at 214 °C ($R_{\text{wp}} = 3.17\%$), (c) $\text{Mg}_{0.5}\text{Mn}_{0.5}(\text{NH}_3)\text{Cl}_2$ at 280 °C ($R_{\text{wp}} = 5.02\%$), and (d) $\text{Mg}_{0.5}\text{Mn}_{0.5}\text{Cl}_2$ at 402 °C ($R_{\text{wp}} = 3.19\%$); showing the experimental (black circles), calculated (solid green line) and the difference plot (solid black line). The vertical ticks mark the Bragg peak positions for the corresponding compounds. $\lambda = 0.82646$ Å. In (a) vertical ticks mark $\text{Mg}_{0.5}\text{Mn}_{0.5}(\text{NH}_3)_6\text{Cl}_2$ (97.6(6) wt%, black) and $\text{Mg}_{0.5}\text{Mn}_{0.5}(\text{NH}_3)_2\text{Cl}_2$ (2.4(5) wt%, red).

Rietveld refinement of $\text{Mg}_{0.5}\text{Mn}_{0.5}(\text{NH}_3)_6\text{Cl}_2$ at RT is performed using the structural model of $\text{Mg}(\text{NH}_3)_6\text{Cl}_2$ (Figure 6a). Two phases are present in the sample, which are identified as $\text{Mg}_{0.5}\text{Mn}_{0.5}(\text{NH}_3)_6\text{Cl}_2$ and $\text{Mg}_{0.5}\text{Mn}_{0.5}(\text{NH}_3)_2\text{Cl}_2$ with the refined phase fractions to 97.6(6) wt% and 2.4(5) wt%, respectively, which might be resulted from partial NH_3 release at RT. $\text{Mg}_{0.5}\text{Mn}_{0.5}(\text{NH}_3)_6\text{Cl}_2$ crystallizes in a cubic unit cell, $a = 10.22037(8)$ Å at RT with space group $Fm-3m$ and is isostructural to $\text{Mg}(\text{NH}_3)_6\text{Cl}_2$. Octahedral $\text{Mg}_{0.5}\text{Mn}_{0.5}(\text{NH}_3)_6$ complexes are contained in a cubic lattice of Cl atoms, with each $\text{Mg}_{0.5}\text{Mn}_{0.5}$ atom octahedrally coordinated by six N atoms.

$\text{Mg}_{0.5}\text{Mn}_{0.5}(\text{NH}_3)_2\text{Cl}_2$ was refined using the $\text{Mg}(\text{NH}_3)_2\text{Cl}_2$ structure as a starting point. Figure 6b shows the Rietveld refinement of the SR-PXD data for $\text{Mg}_{0.5}\text{Mn}_{0.5}(\text{NH}_3)_2\text{Cl}_2$ at 214 °C. For the diammine $\text{Mg}_{0.5}\text{Mn}_{0.5}(\text{NH}_3)_2\text{Cl}_2$, space group $Cmmm$ [43], each Cl atom is shared by two neighboring $\text{Mg}_{0.5}\text{Mn}_{0.5}$ atoms in edge-sharing octahedral chains.

The monoammine $\text{Mg}_{0.5}\text{Mn}_{0.5}(\text{NH}_3)\text{Cl}_2$ is isostructural to $\text{Ni}(\text{NH}_3)\text{Cl}_2$, which crystallizes in a monoclinic unit cell with space group $I2/m$ [44] where each Cl atom is shared by three $\text{Mg}_{0.5}\text{Mn}_{0.5}$ atoms in edge-sharing double octahedral chains. Both broad and narrow diffraction peaks are observed for the monoammine phase (see Figure 6c), indicating the presence of structural disorder or stacking faults in the structure, resulting in a marked difference between the experimental and calculated patterns.

The Rietveld refinement of the fully desorbed $\text{Mg}_{0.5}\text{Mn}_{0.5}\text{Cl}_2$ at 402 °C is shown in Figure 6d. $\text{Mg}_{0.5}\text{Mn}_{0.5}\text{Cl}_2$ structure, space group $R-3m$, is formed by the octahedra of Cl atoms with central $\text{Mg}_{0.5}\text{Mn}_{0.5}$ atoms sharing half of their edges, and thus resulting in layers of $\text{Mg}_{0.5}\text{Mn}_{0.5}\text{Cl}_2$.

Table 2. Structural parameters for the present $\text{Mg}_{0.5}\text{Mn}_{0.5}(\text{NH}_3)_y\text{Cl}_2$ ($y = 6, 2, 1$ and 0) phases investigated in this study.

Chemical Formula	$\text{Mg}_{0.5}\text{Mn}_{0.5}(\text{NH}_3)_6\text{Cl}_2$	$\text{Mg}_{0.5}\text{Mn}_{0.5}(\text{NH}_3)_2\text{Cl}_2$	$\text{Mg}_{0.5}\text{Mn}_{0.5}(\text{NH}_3)\text{Cl}_2$	$\text{Mg}_{0.5}\text{Mn}_{0.5}\text{Cl}_2$
T (°C)	RT	214	280	402
Crystal system	Cubic	Orthorhombic	Monoclinic	Trigonal *
Space group	<i>Fm-3m</i>	<i>Cmmm</i>	<i>I2/m</i>	<i>R-3m</i>
<i>a</i> (Å)	10.22037(8)	8.258(5)	15.575(1)	3.69494(3) Å
<i>b</i> (Å)	-	8.290(4)	3.756(1)	-
<i>c</i> (Å)	-	3.812(2)	14.453(1)	17.8698(4)
β (°)	-	-	106.55(3)	-
<i>V</i> (Å ³)	1067.58(3)	261.0(2)	810.6(9)	211.28(6)
<i>Z</i>	4	2	8	3

* Hexagonal parameters are used in this work.

3.4. NH_3 Cycling and Kinetics

Studies of the NH_3 sorption kinetics and cyclability of the pristine and mixed metal halides with the lower and higher Mn contents ($\text{Mg}_{0.9}\text{Mn}_{0.1}\text{Cl}_2$ and $\text{Mg}_{0.5}\text{Mn}_{0.5}\text{Cl}_2$) were performed using a Sieverts apparatus. The results from the desorption cycles performed on $\text{Mg}_{0.9}\text{Mn}_{0.1}(\text{NH}_3)_6\text{Cl}_2$ are presented in the supporting information (Figure S10). The fifth NH_3 absorption process (after four cycles) of pristine MgCl_2 , MnCl_2 and $\text{Mg}_{0.5}\text{Mn}_{0.5}\text{Cl}_2$ are presented in Figure 7. For absorption, the applied NH_3 gas pressure was ~ 2.5 bar and the processes were conducted at RT. The moles of absorbed NH_3 were calculated (see Equation (1)), where Δn is calculated from the pressure drop, ΔP , occurring during NH_3 absorption. The observed pressure drop was $\Delta P = 0.33$ bar and the final pressures at the end of absorption were 2.21 and 2.22 bar for MgCl_2 and $\text{Mg}_{0.5}\text{Mn}_{0.5}\text{Cl}_2$, respectively. MnCl_2 only absorbed 5.5 moles of NH_3 , which corresponds to a pressure drop of only $\Delta P = 0.29$ bar reaching a final pressure $p = 2.23$ bar. This indicated that not all the MnCl_2 powder had reacted with NH_3 , despite the still relatively high value of the final pressure of absorption. Indeed, due to the large volume expansion of the metal chloride during ammonia absorption, some clogging may occur and prevent ammonia from reaching all the salt crystals [16]. On the other, it cannot be excluded that the absorption reaction stops because the equilibrium pressure for $\text{Mn}(\text{NH}_3)_6\text{Cl}_2$ at RT is higher than the final pressure reached during absorption ($p = 2.23$ bar). A more detailed thermodynamic study using pressure-composition-isotherms is needed to clarify this in detail. MgCl_2 absorbed 6 moles of NH_3 in less than 1000 s, while $\text{Mg}_{0.5}\text{Mn}_{0.5}\text{Cl}_2$ absorbed 6 moles of NH_3 in 6000 s. Similarly, the NH_3 absorption rate for the pristine halides are very different: Four moles of NH_3 is absorbed in MgCl_2 in about 200 s, while it took about 800 s to absorb the similar amount of NH_3 in MnCl_2 . The rate of absorption for $\text{Mg}_{0.5}\text{Mn}_{0.5}\text{Cl}_2$ is similar to that of MnCl_2 , indicating that Mn plays a predominant role for governing the kinetics of the hexammine formation.

The NH_3 desorption processes during cycling were carried out upon heating with a constant heating rate of $2\text{ °C}\cdot\text{min}^{-1}$ from RT to 350 °C under an initial NH_3 pressure of 1 bar, see Figure 8. The moles of desorbed NH_3 were calculated using Equation (1) and the pressure increase, $\Delta P = 0.32$ bar, due to NH_3 release. The three desorption steps of NH_3 were observed as a pressure increase and Δn was calculated. For $\text{Mg}_{0.5}\text{Mn}_{0.5}(\text{NH}_3)_2\text{Cl}_2$, the first 4 moles of NH_3 starts desorbing at around 100 °C and are fully released at 166 °C . The resulting $\text{Mg}_{0.5}\text{Mn}_{0.5}(\text{NH}_3)_2\text{Cl}_2$ desorbs one mole of NH_3 in the temperature range from 240 °C to 260 °C , forming $\text{Mg}_{0.5}\text{Mn}_{0.5}(\text{NH}_3)\text{Cl}_2$. The final NH_3 desorption step occurs above 300 °C . However, the transformation from monoammine to fully desorbed mixed metal chloride, $\text{Mg}_{0.5}\text{Mn}_{0.5}\text{Cl}_2$, does not proceed via a single step as for the previous desorption. Instead it undergoes through two discrete steps, consistent with the observations of a different crystalline phase in the in situ SR-PXD experiments.

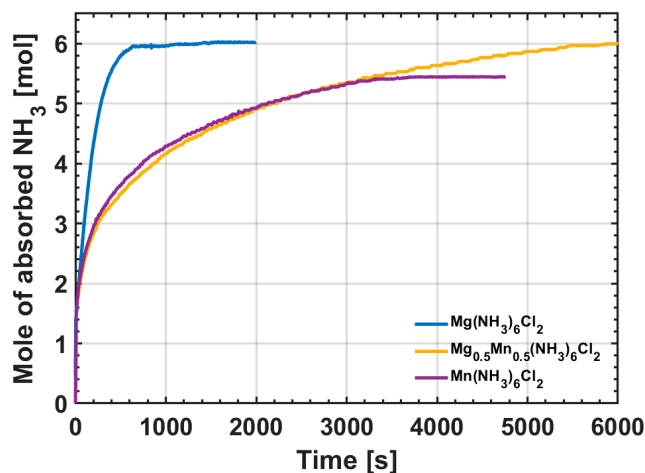


Figure 7. NH_3 absorption processes of $\text{Mg}(\text{NH}_3)_6\text{Cl}_2$ (blue), $\text{Mg}_{0.5}\text{Mn}_{0.5}(\text{NH}_3)_6\text{Cl}_2$ (yellow) and $\text{Mn}(\text{NH}_3)_6\text{Cl}_2$ (purple).

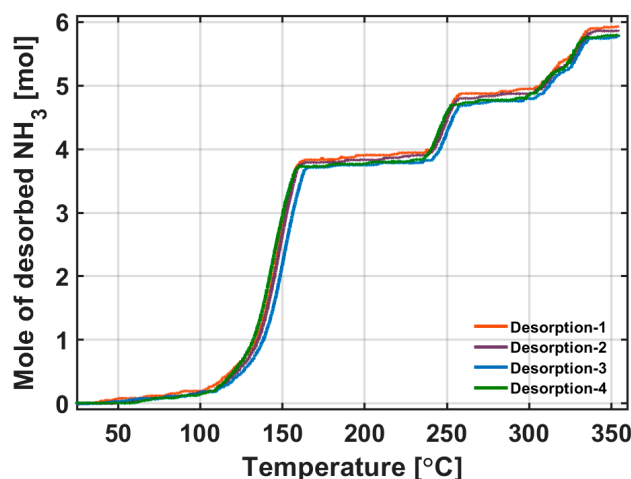


Figure 8. A series of NH_3 desorption from $\text{Mg}_{0.5}\text{Mn}_{0.5}(\text{NH}_3)_6\text{Cl}_2$. The four cycles confirm the stability and cyclability of the mixed metal halide after several ab/desorption cycles.

For some hexammines, $M(\text{NH}_3)_6\text{Cl}_2$ ($M = \text{Mg}, \text{Ni}$), the desorption consists of three events [13]. In contrast, $\text{Mn}(\text{NH}_3)_6\text{Cl}_2$ was reported to undergo non-stoichiometric NH_3 release in the last desorption step [13,42]. In our study, we observe two separate steps, and from the number of desorbed NH_3 moles calculated from ΔP in Sieverts studies, δ seems to be equal to 0.5. Furthermore, the NH_3 desorption studies of $\text{Mg}_{0.9}\text{Mn}_{0.1}(\text{NH}_3)_6\text{Cl}_2$ (Figure S10) suggest that this phenomenon does not occur in $\text{Mg}_{1-x}\text{Mn}_x(\text{NH}_3)_6\text{Cl}_2$ with low Mn content, as the last decomposition step occurs as a single event. This indicates that sufficiently high amount of Mn in $\text{Mg}_{1-x}\text{Mn}_x(\text{NH}_3)_6\text{Cl}_2$ results in a change in the physical behavior to be similar to that of $\text{Mn}(\text{NH}_3)_6\text{Cl}_2$.

These results suggest that by changing the relative Mg:Mn ratio in $\text{Mg}_{1-x}\text{Mn}_x(\text{NH}_3)_6\text{Cl}_2$ the NH_3 sorption properties can be tuned and optimized. For instance, substituting Mg in $\text{Mn}(\text{NH}_3)_6\text{Cl}_2$ increases its stability, avoiding NH_3 desorption at RT. Furthermore, due to the low weight of Mg, the gravimetric capacity increases, with increasing Mg content. Finally, increasing the relative content of magnesium can be beneficial if cost reduction is desirable.

A thorough investigation of the NH_3 desorption reaction enthalpies is planned for further thermodynamic studies of the $\text{Mg}_{1-x}\text{Mn}_x(\text{NH}_3)_6\text{Cl}_2$ hexammines by applying pressure composition isotherm (PCI) studies.

4. Conclusions

A series of novel mixed metal halide ammines, $Mg_{1-x}Mn_x(NH_3)_6Cl_2$, with a usable ammonia capacity in the temperature range 20–350 °C were synthesized and characterized. The crystal structures of the different ammine phases are identified and investigated by in situ SR-PXD. All $Mg_{1-x}Mn_x(NH_3)_6Cl_2$ solid solutions crystallize in a cubic unit cell with space group symmetry $Fm-3m$ and unit cell parameters intermediate that of the two monometallic materials, $Mg(NH_3)_6Cl_2$ and $Mn(NH_3)_6Cl_2$. DSC analysis reveal a decrease in the onset temperature for NH_3 desorption for the solid solutions as compared to the monometallic $Mg(NH_3)_6Cl_2$. Activation energies for each desorption step are calculated and show the possibility of tailoring the activation energies for the NH_3 release in mixed metal chloride hexammines. The lower activation energies for NH_3 desorption in $Mn(NH_3)_6Cl_2$ resulted in a lowering of the activation energies for the solid solution $Mg_{0.5}Mn_{0.5}(NH_3)_6Cl_2$. Finally, NH_3 reversibility measurements reveal that the solid solution has a high stability, thus making them promising candidates for solid-state NH_3 storage systems.

Supplementary Materials: The following are available online at <http://www.mdpi.com/1996-1073/13/11/2746/s1>, Table S1: Structural parameters for the $MgCl_2$, $MnCl_2$ and $Mg_{1-x}Mn_xCl_2$ ($x = 0.025, 0.05, 0.1, 0.3$ and 0.5) solid solutions obtained for this study, Figure S1: Rietveld refinement of SR-PXD data of $Mg(NH_3)_6Cl_2$ at RT, Figure S2: Rietveld refinement of SR-PXD data of $Mg_{0.95}Mn_{0.05}(NH_3)_6Cl_2$ at RT, Figure S3: Rietveld refinement of SR-PXD data of $Mg_{0.9}Mn_{0.1}(NH_3)_6Cl_2$ at RT, Figure S4: Rietveld refinement of SR-PXD data of $Mg_{0.7}Mn_{0.3}(NH_3)_6Cl_2$ at RT, Figure S5: Rietveld refinement of SR-PXD data of $Mn(NH_3)_6Cl_2$ at RT, Figure S6: DSC measurements performed on $Mg(NH_3)_6Cl_2$, $Mn(NH_3)_6Cl_2$ and $Mg_{1-x}Mn_x(NH_3)_6Cl_2$, Table S2: The NH_3 desorption onset temperatures of $Mg(NH_3)_6Cl_2$, $Mn(NH_3)_6Cl_2$ and $Mg_{1-x}Mn_x(NH_3)_6Cl_2$, Table S3: The gravimetric NH_3 capacities of the monometallic and mixed cation hexammines investigated in this study, Figure S7: SR-PXD patterns of $Mg_{1-x}Mn_xCl_2$ after one cycle of NH_3 absorption and desorption, Figure S8: In-situ SR-PXD of $Mg(NH_3)_6Cl_2$ measured from RT to 227 °C, Figure S9: In-situ SR-PXD of $Mn(NH_3)_6Cl_2$ measured from RT to 406 °C, Figure S10: NH_3 desorption upon cycling of $Mg_{0.9}Mn_{0.1}(NH_3)_6Cl_2$.

Author Contributions: Conceptualization, P.B., S.D. and D.B.; methodology, P.B., R.E.J., S.D. and D.B.; formal analysis, P.B., J.B.G. and A.K.; investigation, P.B., J.B.G. and A.K.; resources, D.B. and S.D.; data curation, P.B.; writing—original draft preparation, P.B.; writing—review and editing, A.K., J.B.G., R.E.J., D.B., B.C.H. and S.D.; visualization, P.B.; supervision, B.C.H. and S.D.; project administration, D.B.; funding acquisition, D.B. and S.D. All authors have read and agreed to the published version of the manuscript.

Funding: The Nordic Neutron Science Programme from NordForsk is acknowledged for financial support via the project NHS (No. 82206).

Acknowledgments: J. B. Grinderslev gratefully acknowledges NordForsk for financial support via the NNSP project FunHy (No. 81942). The authors are also grateful to the X04SA beamline at the Swiss light source, Villigen, Switzerland and the local contact Antonio Cervellino for assistance with data collection and the beamline I11 at the Diamond light source, Oxford, UK and the local contacts Stephen Thompson and Chiu Tang for assistance with data collection.

Conflicts of Interest: The authors declare no conflict of interest.

References

1. Mohtadi, R.; Orimo, S. The renaissance of hydrides as energy materials. *Nat. Rev. Mater.* **2016**, *2*, 1–15. [[CrossRef](#)]
2. He, T.; Pachfule, P.; Wu, H.; Xu, Q.; Chen, P. Hydrogen carriers. *Nat. Rev. Mater.* **2016**, *1*, 1–17. [[CrossRef](#)]
3. Milanese, C.; Jensen, T.R.; Hauback, B.C.; Pistidda, C.; Dornheim, M.; Yang, H.; Lombardo, L.; Züttel, A.; Filinchuk, Y.; Ngene, P.; et al. Complex hydrides for energy storage. *Int. J. Hydrog. Energy* **2019**, *44*, 7860–7874. [[CrossRef](#)]
4. Hirscher, M.; Yartys, V.A.; Baricco, M.; Bellosta von Colbe, J.; Blanchard, D.; Bowman, R.C.; Broom, D.P.; Buckley, C.E.; Chang, F.; Chen, P.; et al. Materials for hydrogen-based energy storage—Past, recent progress and future outlook. *J. Alloys Compd.* **2020**, *827*, 153548. [[CrossRef](#)]
5. Zamfirescu, C.; Dincer, I. Ammonia as a green fuel and hydrogen source for vehicular applications. *Fuel Process. Technol.* **2009**, *90*, 729–737. [[CrossRef](#)]
6. Lan, R.; Irvine, J.T.S.; Tao, S. Ammonia and related chemicals as potential indirect hydrogen storage materials. *Int. J. Hydrog. Energy* **2012**, *37*, 1482–1494. [[CrossRef](#)]
7. Zamfirescu, C.; Dincer, I. Using ammonia as a sustainable fuel. *J. Power Sources* **2008**, *185*, 459–465. [[CrossRef](#)]

8. Christensen, C.H.; Johannessen, T.; Sørensen, R.Z.; Nørskov, J.K. Towards an ammonia-mediated hydrogen economy? *Catal. Today* **2006**, *111*, 140–144. [[CrossRef](#)]
9. Makepeace, J.W.; He, T.; Weidenthaler, C.; Jensen, T.R.; Chang, F.; Vegge, T.; Ngene, P.; Kojima, Y.; de Jongh, P.E.; Chen, P.; et al. Reversible ammonia-based and liquid organic hydrogen carriers for high-density hydrogen storage: Recent progress. *Int. J. Hydrog. Energy* **2019**, *44*, 7746–7767. [[CrossRef](#)]
10. Kubota, M.; Matsuo, K.; Yamanouchi, R.; Matsuda, H. Absorption and Desorption Characteristics of NH₃ with Metal Chlorides for Ammonia Storage. *J. Chem. Eng. Jpn.* **2014**. [[CrossRef](#)]
11. Klerke, A.; Christensen, C.H.; Nørskov, J.K.; Vegge, T. Ammonia for hydrogen storage: Challenges and opportunities. *J. Mater. Chem.* **2008**, *18*, 2304–2310. [[CrossRef](#)]
12. Christensen, C.H.; Sørensen, R.Z.; Johannessen, T.; Quaade, U.J.; Honkala, K.; Elmøe, T.D.; Køhler, R.; Nørskov, J.K. Metal ammine complexes for hydrogen storage. *J. Mater. Chem.* **2005**, *15*, 4106–4108. [[CrossRef](#)]
13. Sørensen, R.Z.; Hummelshøj, J.S.; Klerke, A.; Reves, J.B.; Vegge, T.; Nørskov, J.K.; Christensen, C.H. Indirect, Reversible High-Density Hydrogen Storage in Compact Metal Ammine Salts. *J. Am. Chem. Soc.* **2008**, *130*, 8660–8668. [[CrossRef](#)] [[PubMed](#)]
14. Jacobsen, H.S.; Hansen, H.A.; Andreasen, J.W.; Shi, Q.; Andreasen, A.; Feidenhans'l, R.; Nielsen, M.M.; Ståhl, K.; Vegge, T. Nanoscale structural characterization of Mg(NH₃)₆Cl₂ during NH₃ desorption: An in situ small angle X-ray scattering study. *Chem. Phys. Lett.* **2007**, *441*, 255–260. [[CrossRef](#)]
15. Walker, G. *Solid-State Hydrogen Storage: Materials and Chemistry*; Woodhead Publishing: Cambridge, UK, 2008; ISBN 978-1-84569-494-4.
16. Tekin, A.S.; Hummelshøj, J.S.; Jacobsen, H.; Sveinbjörnsson, D.; Blanchard, D.K.; Nørskov, J.; Vegge, T. Ammonia dynamics in magnesium ammine from DFT and neutron scattering. *Energy Environ. Sci.* **2010**, *3*, 448–456. [[CrossRef](#)]
17. Elmøe, T.D.; Sørensen, R.Z.; Quaade, U.; Christensen, C.H.; Nørskov, J.K.; Johannessen, T. A high-density ammonia storage/delivery system based on Mg(NH₃)₆Cl₂ for SCR–DeNO_x in vehicles. *Chem. Eng. Sci.* **2006**, *61*, 2618–2625. [[CrossRef](#)]
18. Hwang, I.C.; Drews, T.; Seppelt, K. Mg(NH₃)₆Hg₂₂, a Mercury Intercalation Compound. *J. Am. Chem. Soc.* **2000**, *122*, 8486–8489. [[CrossRef](#)]
19. Wentworth, W.E.; Raldow, W.M.; Corbett, G.E. Correlation of thermodynamic properties for dissociation of amines of divalent metal halides. *Inorg. Chim. Acta* **1978**, *30*, L299–L301. [[CrossRef](#)]
20. Bevers, E.; Oonk, H.; Haije, W.; van Ekeren, P. Investigation of thermodynamic properties of magnesium chloride amines by HPDSC and TG. *J. Therm. Anal. Calorim.* **2007**, *90*, 923–929. [[CrossRef](#)]
21. Aoki, T.; Miyaoka, H.; Inokawa, H.; Ichikawa, T.; Kojima, Y. Activation on Ammonia Absorbing Reaction for Magnesium Chloride. *J. Phys. Chem. C* **2015**, *119*, 26296–26302. [[CrossRef](#)]
22. Aoki, T.; Ichikawa, T.; Miyaoka, H.; Kojima, Y. Thermodynamics on Ammonia Absorption of Metal Halides and Borohydrides. *J. Phys. Chem. C* **2014**, *118*, 18412–18416. [[CrossRef](#)]
23. Eßmann, R.; Kreiner, G.; Niemann, A.; Rechenbach, D.; Schmieding, A.; Sichla, T.; Zachwieja, U.; Jacobs, H. Isotype Strukturen einiger Hexaamminmetall(II)-halogenide von 3d-Metallen: [V(NH₃)₆]I₂, [Cr(NH₃)₆]I₂, [Mn(NH₃)₆]Cl₂, [Fe(NH₃)₆]Cl₂, [Fe(NH₃)₆]Br₂, [Co(NH₃)₆]Br₂ und [Ni(NH₃)₆]Cl₂. *Z. Anorg. Allg. Chem.* **1996**, *622*, 1161–1166. [[CrossRef](#)]
24. Lysgaard, S.; Ammitzbøll, A.L.; Johnsen, R.E.; Norby, P.; Quaade, U.J.; Vegge, T. Resolving the stability and structure of strontium chloride amines from equilibrium pressures, XRD and DFT. *Int. J. Hydrog. Energy* **2012**, *37*, 18927–18936. [[CrossRef](#)]
25. Bialy, A.; Jensen, P.B.; Blanchard, D.; Vegge, T.; Quaade, U.J. Solid solution barium–strontium chlorides with tunable ammonia desorption properties and superior storage capacity. *J. Solid State Chem.* **2015**, *221*, 32–36. [[CrossRef](#)]
26. Kishida, Y.; Aoki, M.; Yamauchi, T. Crystal Structure and NH₃ Desorption Properties of Complex Metal Ammine Chloride. *J. Chem. Eng. Jpn.* **2019**, *52*, 239–242. [[CrossRef](#)]
27. Lasocha, W.; Eick, H.A. The structure of Ca_{0.3}Sr_{0.7}Cl₂ and Ca_{0.46}Sr_{0.54}Cl₂ by the X-ray Rietveld refinement procedure. *J. Solid State Chem.* **1988**, *75*, 175–182. [[CrossRef](#)]
28. Liu, C.Y.; Aika, K. Ammonia Absorption into Alkaline Earth Metal Halide Mixtures as an Ammonia Storage Material. *Ind. Eng. Chem. Res.* **2004**, *43*, 7484–7491. [[CrossRef](#)]
29. Hodorowicz, S.A.; Eick, H.A. Phase relationships in the system SrBr₂–SrCl₂. *J. Solid State Chem.* **1982**, *43*, 271–277. [[CrossRef](#)]

30. Hodorowicz, S.A.; Eick, H.A. An X-ray diffraction study of the $\text{SrBr}_x\text{I}_{2-x}$ system. *J. Solid State Chem.* **1983**, *46*, 313–320. [[CrossRef](#)]
31. Černý, R.; Penin, N.; D'Anna, V.; Hagemann, H.; Durand, E.; Růžička, J. $\text{Mg}_x\text{Mn}_{(1-x)}(\text{BH}_4)_2$ ($x=0-0.8$), a cation solid solution in a bimetallic borohydride. *Acta Mater.* **2011**, *59*, 5171–5180. [[CrossRef](#)]
32. Jepsen, L.H.; Ley, M.B.; Filinchuk, Y.; Besenbacher, F.; Jensen, T.R. Tailoring the Properties of Ammine Metal Borohydrides for Solid-State Hydrogen Storage. *ChemSusChem* **2015**, *8*, 1452–1463. [[CrossRef](#)] [[PubMed](#)]
33. Kissinger, H.E. Variation of Peak Temperature with Heating Rate in Differential Thermal Analysis. *J. Res. Natl. Bur. Stand.* **1956**, *57*, 217–221. [[CrossRef](#)]
34. Willmott, P.R.; Meister, D.; Leake, S.J.; Lange, M.; Bergamaschi, A.; Böge, M.; Calvi, M.; Cancellieri, C.; Casati, N.; Cervellino, A.; et al. The Materials Science beamline upgrade at the Swiss Light Source. *J. Synchrotron. Radiat.* **2013**, *20*, 667–682. [[CrossRef](#)] [[PubMed](#)]
35. Thompson, S.P.; Parker, J.E.; Potter, J.; Hill, T.P.; Birt, A.; Cobb, T.M.; Yuan, F.; Tang, C.C. Beamline I11 at Diamond: A new instrument for high resolution powder diffraction. *Rev. Sci. Instrum.* **2009**, *80*, 075107. [[CrossRef](#)] [[PubMed](#)]
36. Pathak, P.D.; Vasavada, N.G. Thermal expansion of NaCl, KCl and CsBr by X-ray diffraction and the law of corresponding states. *Acta Crystallogr. A* **1970**, *26*, 655–658. [[CrossRef](#)]
37. Coelho, A.A. TOPAS and TOPAS-Academic: An optimization program integrating computer algebra and crystallographic objects written in C++. *J. Appl. Crystallogr.* **2018**, *51*, 210–218. [[CrossRef](#)]
38. Tornero, J.D.; Fayos, J. Single crystal structure refinement of MnCl_2 . *Z. Krist.* **2015**, *192*, 147–148. [[CrossRef](#)]
39. Feitknecht, W.; Held, F. Über die Hydroxychloride des Magnesiums. *Helv. Chim. Acta* **1944**, *27*, 1480–1495. [[CrossRef](#)]
40. Shannon, R.D. Revised effective ionic radii and systematic studies of interatomic distances in halides and chalcogenides. *Acta Crystallogr. A* **1976**, *32*, 751–767. [[CrossRef](#)]
41. King, H.W. Quantitative size-factors for metallic solid solutions. *J. Mater. Sci.* **1966**, *1*, 79–90. [[CrossRef](#)]
42. Reardon, H.; Hanlon, J.M.; Grant, M.; Fullbrook, I.; Gregory, D.H. Ammonia Uptake and Release in the $\text{MnX}_2\text{-NH}_3$ ($X = \text{Cl}, \text{Br}$) Systems and Structure of the $\text{Mn}(\text{NH}_3)_n\text{X}_2$ ($n = 6, 2$) Ammines. *Crystals* **2012**, *2*, 193–212. [[CrossRef](#)]
43. Leineweber, A.; Friedriszik, M.W.; Jacobs, H. Preparation and Crystal Structures of $\text{Mg}(\text{NH}_3)_2\text{Cl}_2$, $\text{Mg}(\text{NH}_3)_2\text{Br}_2$, and $\text{Mg}(\text{NH}_3)_2\text{I}_2$. *J. Solid State Chem.* **1999**, *147*, 229–234. [[CrossRef](#)]
44. Leineweber, A.; Jacobs, H.; Ehrenberg, H. Crystal Structure of $\text{Ni}(\text{NH}_3)\text{Cl}_2$ and $\text{Ni}(\text{NH}_3)\text{Br}_2$. *Z. Anorg. Allg. Chem.* **2000**, *626*, 2146–2152. [[CrossRef](#)]

